PHYSICAL REVIEW E **72**, 010401(R) (2005)

# Interactions between nanoparticles in supercritical fluids: From repulsion to attraction

S. A. Egorov
*Department of Chemistry, University of Virginia, Charlottesville, Virginia 22901, USA*
(Received 5 January 2005; revised manuscript received 7 March 2005; published 15 July 2005)

We present a density functional theory study of interactions between sterically stabilized spherical nanoparticles in a supercritical solvent. The theory is used to analyze the effect of particle size, solvent density, and solvent-ligand interaction strength on the potential of mean force between the particles. Experimentally observed size-selective precipitation of nanoparticles is rationalized in terms of the behavior of the density profiles of stabilizing ligands as a function of particle size and solvent thermodynamic conditions. The theory yields the same general trends as observed in experiments, namely, an increased stability of nanoparticle dispersions at higher solvent densities and for smaller particle sizes.

DOI: 10.1103/PhysRevE.72.010401 PACS number(s): 82.70.Dd, 61.46.+w, 64.70.Fx, 83.80.Hj

Particles with dimensions in the range of 20–100 Å are characterized by unique size-dependent optical, electronic, and magnetic properties that could be useful for a variety of technologies including coating, catalysis, memory, and sensor applications [1–4]. Given the strong size dependence of various nanoparticle properties, it is crucial to be able to prepare nanocrystals with *narrow size distribution*. One of the most successful methods involves arrested precipitation, which relies on the use of organic ligands for the purpose of passivating the surfaces of nanoparticles during growth in order to provide size control and protection against irreversible aggregation [5]. A particularly versatile implementation of this procedure employs highly compressible supercritical fluids (SCFs) as tunable solvents for nanomaterials processing [6–8]. The unique advantage provided by SCFs is their easily adjustable density, and, hence, solvating ability [9,10], which makes it possible to control the nanoparticle interactions through the extent of solvation of stabilizing ligands.

In a recent experimental study, silver and gold nanocrystals sterically stabilized with dodecanethiol ligands were dispersed in supercritical ethane [8]. Their dispersibility was shown to be strongly dependent on the nanocrystal *size* and the solvent *density*. The lowering of ethane density decreases ligand solvation, thereby reducing steric stabilization and leading to flocculation of nanocrystals, with precipitation of larger particles occurring at better solvent conditions (higher density) compared to smaller particles, which allows the preparation of relatively monodisperse nanocrystals [8].

On the theoretical side, both computer simulations [11] and lattice fluid self-consistent field theory [12,13] have demonstrated the collapse of grafted stabilizing ligands with decreasing solvent density and the concomitant change in the nature of the interaction between passivated particles from repulsive to attractive. However, these studies were performed for *flat noninteracting* walls with end-grafted polymers, while the analysis of *size-selective* nanocrystal preparation requires the consideration of *spherical interacting* particles, whose size affects both the core-core interaction strength (van der Waals-like term) and the density profile of stabilizing ligands [8]. In particular, the ability of the latter to move out of the way (as two particles approach each other) strongly depends on the curvature of the core [14,15]. While the dependence of the van der Waals term on the particle radius is well understood [16], the analysis of a polymer mediated component as a function of the core radius is more challenging. In fact, a recent self-consistent field study has shown that spherical nanoparticles with end-grafted polymeric stabilizers can experience a polymer-induced attractive interaction even under *good solvent* conditions, which is in stark contrast to the case of flat walls [15]. Given that in the systems studied experimentally the sizes of nanoparticle cores and stabilizing ligands are comparable [8], it is crucial to include this aspect into theoretical analysis.

Due to the lower symmetry of the problem, theoretical treatments of interactions between spherical brushes are more demanding compared to well-studied flat brushes, and only a few calculations have been reported, based either on scaling arguments [17] or on self-consistent field theory [14,15]. However, all these studies were limited to good solvent conditions and no explicit solvent was considered, so that their results are not directly applicable to the analysis of experiments carried out in SCFs, with their strong density inhomogeneities and highly tunable solvent quality [9,10]. In principle, the interactions between passivated nanoparticles in a supercritical solvent can be obtained directly from computer simulations. Unfortunately, such simulations for spherical nanoparticles are again much more demanding (compared to flat brushes [11]) due to the need for a much larger simulation box that would require simulating many thousands of solvent molecules. Indeed, a recent detailed atomistic simulation study of solvation of gold nanoparticles stabilized with alkanethiol chains in supercritical ethane was limited to a single nanoparticle, so that no interactions were computed [18].

In view of the above, it would be advantageous to develop a theoretical method that would permit an efficient calculation of the interaction between sterically stabilized nanoparticles in an explicit solvent, while describing the end-grafted polymers at a proper level of microscopic detail (similar to the level achieved in atomistic simulations). Namely, the stabilizers need to be treated as connected chains of monomeric units that experience both steep repulsions and soft attractions among themselves, with the solvent molecules, and with the nanoparticle cores. In this Rapid Communication, we propose such a method on the basis of the classical density functional theory (DFT). Specifically, we employ the version of the DFT recently formulated by Muller, Macdowell, and Yethiraj [19], which is designed for treating systems

 

where both hard-core repulsive and soft attractive interactions are present. This method has been already applied to study interactions between bare (nonpassivated) nanoparticles in a hard-core Yukawa fluid [20], and was shown to be in quantitative agreement with the available simulation data [21]. In the present paper, we extend the method to treat the nanoparticles with end-grafted polymers, and study the interactions between passivated particles as a function of solvent density and particle size. Our primary goal is to rationalize the experimental observation that the flocculation of larger nanoparticles occurs at higher solvent densities compared to smaller ones, which is the key to size-selective preparation.

The quantity of major interest for us is the potential of mean force (PMF) between the two particles, which governs the stability of the nanoparticle dispersions: as the PMF well depth drops below $-3k_BT/2$, the dispersion becomes unstable and flocculation occurs [7]. The total PMF between two passivated nanoparticles in solution, $\Phi(r)$, is composed of the bare core-core interaction, $\phi_{cc}(r)$, and the solvent-polymer mediated component, $W(r)$. While both terms depend on the core size, only the latter is controlled by the solvent thermodynamic conditions.

As our microscopic model, we consider two spherical particles of diameter $\sigma_{cc}$, each uniformly composed of Lennard-Jones (LJ) spheres with diameter $\sigma$, well depth $\epsilon$, and number density $\rho$ [22]. These spherical cores are grafted with $N_{ch}$ fully flexible polymer chains composed of $N_p$ tangent spherical segments with diameter $\sigma_{pp}$. The two brushes are immersed in a fluid of spherical particles with diameter $\sigma_{ss}$.

The bare interaction potential, $\phi_{cc}(r)$, is obtained by integrating the individual LJ interactions over the volume of nanoparticles [22]; the resulting form is rather lengthy and will not be reproduced here [it is important to note that $\phi_{cc}(r)$ contains both a van der Waals-type attraction and a short-range repulsion]. We further assume that all solvent particles and nonbonded chain segments interact with each other and with the nanoparticle core via isotropic potential of the hard-core Yukawa form: $v_{ij}(r)=\epsilon_{ij}\sigma_{ij}\exp[-\kappa_{ij}(r-\sigma_{ij})]/r$ for $r\geqslant\sigma_{ij}$ and $v_{ij}(r)=\infty$ for $r<\sigma_{ij}$, where $\sigma_{ij}=(\sigma_{ii}+\sigma_{jj})/2$, and $i,j=s,p,c$, which stand for the solvent, the polymer segment, and the nanoparticle core, respectively. The intramolecular chain potential (in addition to the nonbonded energy $\Sigma_{i=3}^{N_p}\Sigma_{j=1}^{i-2}v_{pp}(|\mathbf{r}_i-\mathbf{r}_j|)$), includes the bonding term $V_b(\mathbf{R}_p)$ defined by $\exp[-\beta V_b(\mathbf{R}_p)]=\Pi_{i=1}^{N_p-1}\delta(|\mathbf{r}_i-\mathbf{r}_{i+1}|-\sigma_{pp})/(4\pi\sigma_{pp}^2)$, where $\beta=1/k_BT$, $\mathbf{r}_i$ are the positions of the polymer beads, and $\mathbf{R}_p=\{\mathbf{r}_i\}$. Finally, the innermost ($i=1$) bead is tethered to the nanoparticle core via the grafting potential $\exp[-\beta v_{cp}(\mathbf{r}_1)]=\delta(r_1-\sigma_{cp})/(4\pi\sigma_{cp}^2)$.

In order to obtain $W(R)$, we define $\rho_s(\mathbf{r},R)$ ($\rho_p(\mathbf{r},R)$) as the conditional probability of finding a solvent particle (polymer segment) at $\mathbf{r}$ given that one nanoparticle is at the origin and the other is located at $\vec{R}$. With this definition, the solvent-polymer mediated PMF between the two nanoparticles can be obtained as $W(R)=\int_R^\infty F(R')dR'$, where the excess mean force is given by [23,24]

$$F(R)=-\int d\mathbf{r}[(\nabla v_{cs}(r)\cdot\hat{\mathbf{R}})\rho_s(\mathbf{r};R)+(\nabla v_{cp}(r)\cdot\hat{\mathbf{R}})\rho_p(\mathbf{r};R)]. \tag{1}$$

By treating the two nanoparticles as a source of an external field, we can employ the standard DFT formalism to obtain the equilibrium density profile of the fluid and polymer segments in an external potential, and thus compute $W(R)$.

The DFT method for hard-sphere Yukawa fluid has been detailed in Ref. [20]; here we briefly summarize the main points and focus on features associated with end-grafted polymers. The starting point is the expression for the grand free energy functional, which is related to the Helmholtz free energy functional via a Legendre transform:

$$\Omega=F[\rho_s(\mathbf{r}),\rho_p(\mathbf{R}_p)]+\int d\mathbf{R}_p\rho_p(\mathbf{R}_p)[V_{cp}(\mathbf{R}_p)-\mu_p]+\int d\mathbf{r}\rho_s(\mathbf{r})[V_{cs}(\mathbf{r})-\mu_s],$$

where $\mu_s$ ($\mu_p$) is the solvent (polymer) chemical potential, and $V_{cs}$ ($V_{cp}$) is the external field exerted by nanoparticle cores on the solvent (polymer). The Helmholtz functional is separated into ideal and excess parts [19,25], with the former given by

$$\beta F_{id}[\rho_s(\mathbf{r}),\rho_p(\mathbf{R}_p)]=\int d\mathbf{R}_p\rho_p(\mathbf{R}_p)[\ln\rho_p(\mathbf{R}_p)-1]+\beta\int d\mathbf{R}_p\rho_p(\mathbf{R}_p)V_b(\mathbf{R}_p)+\int d\mathbf{r}\rho_s(\mathbf{r})\times[\ln\rho_s(\mathbf{r})-1], \tag{2}$$

while the latter is computed in the weighted density approximation [25]

$$F_{ex}[\rho_s(\mathbf{r}),\rho_p(\mathbf{r})]=\int d\mathbf{r}\{\rho_p(\mathbf{r})[f_p^r(\bar{\rho}_r(\mathbf{r}))+f_p^a(\bar{\rho}_a(\mathbf{r}))]+\rho_s(\mathbf{r})\times[f_s^r(\bar{\rho}_r(\mathbf{r}))+f_s^a(\bar{\rho}_a(\mathbf{r}))]\}, \tag{3}$$

where $f_i^{r/a}$ is the repulsive (attractive) contribution to the excess free energy density per site of species $i$, and $\bar{\rho}_{r/a}$ is the total (segment plus solvent) weighted density: $\bar{\rho}_{r/a}(\mathbf{r})=\int d\mathbf{r}'[\rho_s(\mathbf{r}')+\rho_p(\mathbf{r}')]w_{r/a}(|\mathbf{r}-\mathbf{r}'|)$, with weighting functions $w_{r/a}$ normalized to unity. The expressions for $w_{r/a}$ and $f_s^{r/a}$ were given earlier [20,26]; $f_p^{r/a}$ for Yukawa chains are obtained from the thermodynamic perturbation theory [27]

Minimization of $\Omega$ with respect to $\rho_p(\mathbf{R}_p)$ yields the equilibrium polymer density distribution, which can be integrated over grafting and bonding delta functions to obtain the following result for the $i$th segment density profile:

$$\rho_{pi}(\mathbf{r}_i)=C_iI(\mathbf{r}_i)I_i^-(\mathbf{r}_i)I_i^+(\mathbf{r}_i),$$

$$I(\mathbf{r})=\exp[-\beta(v_{cp}(\mathbf{r})+v_{cp}(|\mathbf{r}-\mathbf{R}|)+\lambda_p(\mathbf{r}))], \tag{4}$$

where

$$\lambda_p(\mathbf{r}) = f_p^r(\bar{\rho}_r(\mathbf{r})) + f_p^a(\bar{\rho}_a(\mathbf{r})) + \gamma_p^r(\mathbf{r}) + \gamma_p^a(\mathbf{r}) + \gamma_s^r(\mathbf{r}) + \gamma_s^a(\mathbf{r}),$$

and

$$\gamma_i^{r/a}(\mathbf{r}) = \int d\mathbf{r}' \rho_i(\mathbf{r}') w_{r/a}(|\mathbf{r}-\mathbf{r}'|) df_i^{r/a}[\bar{\rho}(\mathbf{r}')]/d\rho.$$

The normalization constant $C_i$ is chosen to ensure that the density profile is normalized to $N_{ch}$.

The two propagators in Eq. (4), $I_i^+$ and $I_i^-$ move from the free ($i=N_p$) and the tethered ($i=1$) ends of the chain, respectively. The former is given by

$$I_i^+(\mathbf{r}) = \frac{1}{4\pi\sigma_{pp}^2} \int d\mathbf{r}' \delta(|\mathbf{r}-\mathbf{r}'| - \sigma_{pp}) I(\mathbf{r}') I_{i+1}^+(\mathbf{r}'),$$

$$I_{N_p}^+(\mathbf{r}) = 1. \quad (5)$$

In order to ensure the uniform distribution of $N_{ch}$ grafted segments on the surface of the sphere of radius $\sigma_{cp}$, we set the value of $I_1^-$ at the core radius to

$$I_1^-(|\mathbf{r}| = \sigma_{cp}) = \frac{\delta(r-\sigma_{cp})}{4\pi\sigma_{cp}^2} \frac{N_{ch}}{I_1^+(|\mathbf{r}| = \sigma_{cp}) I(|\mathbf{r}| = \sigma_{cp})}. \quad (6)$$

$I_i^-$ for the remaining segments is obtained from iterative relation similar to Eq. (5).

Minimizing $\Omega$ with respect to $\rho_s(\mathbf{r})$ yields the equilibrium solvent density distribution

$$\rho_s(\mathbf{r}) = \exp[-\beta(v_{cs}(\mathbf{r}) + v_{cs}(|\mathbf{r}-\mathbf{R}|) + \lambda_s(\mathbf{r}) - \mu_s)], \quad (7)$$

where

$$\lambda_s(\mathbf{r}) = f_s^r(\bar{\rho}_r(\mathbf{r})) + f_s^a(\bar{\rho}_a(\mathbf{r})) + \gamma_p^r(\mathbf{r}) + \gamma_p^a(\mathbf{r}) + \gamma_s^r(\mathbf{r}) + \gamma_s^a(\mathbf{r}).$$

The coupled Eqs. (4) and (7) are solved iteratively on $(r, \theta)$ grid by expanding the functions in Legendre polynomials, as described in detail in Ref. [20].

In choosing potential parameters for our model calculations, we are guided by the experimental study [8] involving alkanes as stabilizing chains and ethane as supercritical solvent, wherein ligand segments and solvent particles are similar in chemical nature. For simplicity, we set segment-segment, segment-solvent, and solvent-solvent interaction potentials to be identical: $\sigma_{pp}=\sigma_{ss}$, $\epsilon_{pp}=\epsilon_{ss}=\epsilon_{ps}$, and $\kappa_{pp}=\kappa_{ss}=\kappa_{ps}=3.0/\sigma_{ss}$. Likewise, we choose the core-segment and core-solvent interactions to be identical, i.e., there is no preferential solvation of the nanoparticle cores by either monomers or solvent particles: $\epsilon_{cp}=\epsilon_{cs}=0.82\epsilon_{ss}$, and $\kappa_{cp}=\kappa_{cs}=1.2/\sigma_{ss}$. The parameters for $\phi_{cc}(r)$ are taken as follows [22]: $\sigma=\sigma_{ss}$, $\rho\sigma^3=1$, and $\epsilon=\epsilon_{ss}/4$.

Thermodynamic conditions of the solvent are determined by its bulk density and temperature, which we define in dimensionless form: $\rho_b^*=\rho_b\sigma_{ss}^3$ and $T^*=k_BT/\epsilon_{ss}$. The critical parameters for our Yukawa solvent are [28]: $\rho_{bc}^*=0.375$ and $T_c^*=0.715$. We focus on the supercritical isotherm $T^*=1.0$ and compute the PMF between nanoparticles at the following three solvent densities: $\rho_b^*=0.2$, 0.3, and 0.45. We start by considering two sterically stabilized particles with core diameters $\sigma_{cc}=5\sigma_{ss}$, $N_{ch}=10$, and $N_p=20$. Our results for the total PMF at three densities are shown in the upper panel of Fig. 1 (along with the bare core-core term). One sees that at the highest density $\Phi(r)$ is largely repulsive, with a very shallow attractive well at large separations. As the density is lowered, $\Phi(r)$ becomes more attractive, and at $\rho_b^*=0.3$ the well depth drops just below $-3k_BT/2$, marking the onset of flocculation. At the lowest density, the PMF well is more than twice as deep.

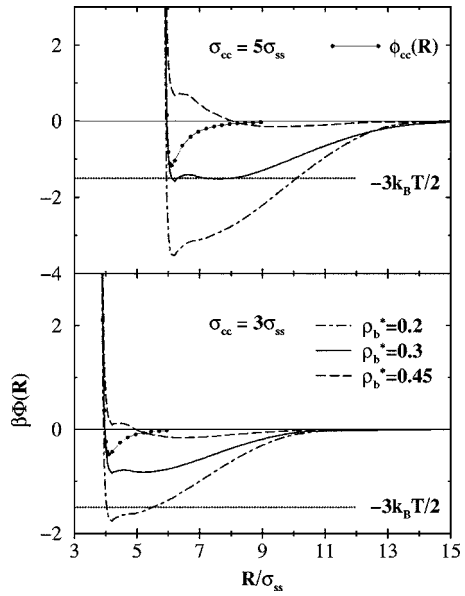


FIG. 1. Potentials of mean force between sterically stabilized nanoparticles at three values of the solvent density (other parameters are described in the text).

By integrating the two terms in Eq. (1) separately, we decompose $W(R)$ into solvent- $[W_s(R)]$ and polymer- $[W_p(R)]$ induced components, which are shown in Fig. 2. One sees that the density dependence of the PMF is dominated by the polymer-induced term (the solvent-induced term is primarily repulsive and rather weakly varying with $\rho_b$,

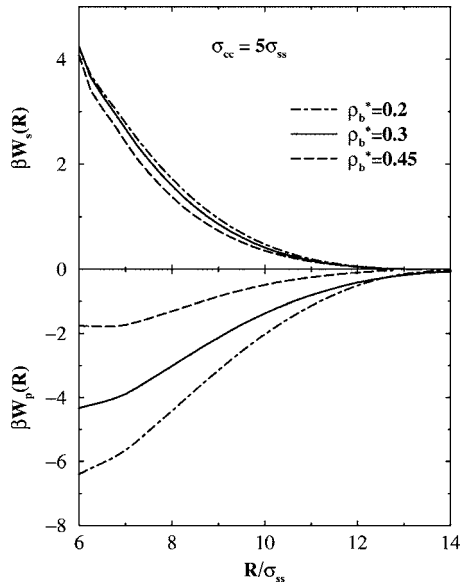


FIG. 2. Solvent (upper panel) and polymer (lower panel) mediated components of the potential of mean force between two sterically stabilized nanoparticles.

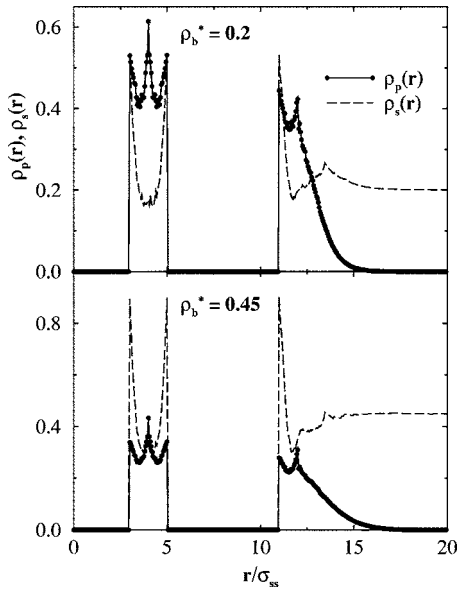


FIG. 3. Polymer and solvent density profiles for a given separation between the nanoparticles at two values of the solvent density.

similar to the case of bare nanoparticles [20]). In order to rationalize this result, we have plotted in Fig. 3 the polymer and solvent density profiles along the line connecting the two nanoparticle centers at the separation $R=8\sigma_{ss}$. The upper and lower panels show the results for $\rho_b^*=0.2$ and 0.45, respectively. At the low density point, the stabilizing ligands are poorly solvated, and the *chain segments* cluster in the region between the two cores, forming a locally dense region that creates a bridging attraction between the two particles [29]. At the higher density, the chains are adequately solvated and more extended into the solvent, which causes the bridging attraction to weaken, while steric repulsion increases, resulting in a primarily repulsive total PMF (for a single nanoparticle, the mean-squared distance for the chain-ending segment from the particle center increases by $\sim 50\%$, from $29\sigma_{ss}^2$ at $\rho_b^*=0.2$ to $44\sigma_{ss}^2$ at $\rho_b^*=0.45$).

Next, we consider a smaller nanoparticle with $\sigma_{cc}=3\sigma_{ss}$ and the same coverage as the larger one. The corresponding results for $\Phi(R)$ at three solvent densities are shown in the lower panel of Fig. 1. In accordance with experimental observations, the onset of flocculation occurs at a lower solvent density ($\rho_b^* \sim 0.2$) compared to the larger core. While the well depth of the bare potential $\phi_{cc}$ does diminish with core size [8], the dominant size effect comes from the polymer-induced component of the PMF. The segment density as a function of distance from the core decays faster for smaller particles, which reduces both bridging attraction and steric repulsion. Overall, the former effect wins over the latter at lower solvent densities, which results in a less attractive PMF for a smaller particle.

In conclusion, we have proposed an efficient approach for computing interactions between sterically stabilized spherical nanoparticles in an explicit solvent. Our model calculations have successfully reproduced several experimentally observed trends, namely increasing the stability of nanoparticle dispersions at higher SCF densities, as well as a greater dispersibility of smaller particles at given solvent conditions.

The author acknowledges numerous helpful discussions of DFT with Professor Arun Yethiraj. The author is grateful for financial support from the National Science Foundation through Grant No. CHE-0235768.

[1] A. P. Alivisatos, Science **271**, 933 (1996).
[2] A. P. Alivisatos, J. Phys. Chem. **100**, 13226 (1996).
[3] Y. Wang, Acc. Chem. Res. **24**, 133 (1991).
[4] C. B. Murray, D. J. Norris, and M. G. Bawendi, J. Am. Chem. Soc. **115**, 8706 (1993).
[5] B. A. Korgel, S. Fullam, S. Connolly, and D. Fitzmaurice, J. Phys. Chem. B **102**, 8379 (1998).
[6] K. P. Johnston and P. S. Shah, Science **303**, 482 (2004).
[7] P. S. Shah, T. Hanrath, K. P. Johnston, and B. A. Korgel, J. Phys. Chem. B **108**, 9574 (2004).
[8] P. S. Shah, J. D. Holmes, K. P. Johnston, and B. A. Korgel, J. Phys. Chem. B **106**, 2545 (2002).
[9] S. A. Egorov, A. Yethiraj, and J. L. Skinner, Chem. Phys. Lett. **317**, 558 (2000).
[10] S. A. Egorov, Phys. Rev. Lett. **93**, 023004 (2004).
[11] J. C. Meredith, I. C. Sanchez, K. P. Johnston, and J. J. dePablo, J. Chem. Phys. **109**, 6424 (1998).
[12] J. C. Meredith and K. P. Johnston, Macromolecules **31**, 5507 (1998).
[13] J. C. Meredith and K. P. Johnston, Macromolecules **31**, 5518 (1998).
[14] C. M. Wijmans, F. A. M. Leermakers, and G. J. Fleer, Langmuir **10**, 4514 (1994).
[15] J. R. Roan, Phys. Rev. Lett. **86**, 1027 (2001).
[16] H. C. Hamaker, Physica (Amsterdam) **4**, 1058 (1937).
[17] T. A. Whitten and P. A. Pincus, Macromolecules **19**, 2509 (1986).
[18] M. Lal, M. Plummer, N. J. Richmond, and W. Smith, J. Phys. Chem. B **108**, 6052 (2004).
[19] M. Müller, L. G. MacDowell, and A. Yethiraj, J. Chem. Phys. **118**, 2929 (2003).
[20] S. A. Egorov, Phys. Rev. E **70**, 031402 (2004).
[21] A. A. Louis, E. Allahyarov, H. Löwen, and R. Roth, Phys. Rev. E **65**, 061407 (2002).
[22] E. Rabani and S. A. Egorov, J. Phys. Chem. B **106**, 6771 (2002).
[23] A. Jusufi, M. Watzlawek, and H. Lowen, Macromolecules **32**, 4470 (1999).
[24] J. Liu and E. Luijten, Phys. Rev. Lett. **93**, 247802 (2004).
[25] A. Yethiraj and C. E. Woodward, J. Chem. Phys. **102**, 5499 (1995).
[26] D. M. Duh and L. Mier-Y-Teran, Mol. Phys. **90**, 373 (1997).
[27] L. A. Davies, A. Gil-Villegas, and G. Jackson, J. Chem. Phys. **111**, 8659 (1999).
[28] E. Lomba and N. G. Almarza, J. Chem. Phys. **100**, 8367 (1994).
[29] J. Yaneva, A. Milchev, and K. Binder, J. Chem. Phys. **121**, 12632 (2004).